



# Magnetic nanoparticles in different biological environments analyzed by magnetic particle spectroscopy



Norbert Löwa\*, Maria Seidel, Patricia Radon, Frank Wiekhorst

Physikalisch-Technische Bundesanstalt, Abbestr. 2-12, 10587 Berlin, Germany

## ARTICLE INFO

### Keywords:

Nanoparticles  
Magnetic particle spectroscopy  
Quantification  
Colloidal stability  
Magnetic particle imaging

## ABSTRACT

Quantification of magnetic iron oxide nanoparticles (MNP) in biological systems like cells, tissue, or organs is of vital importance for development of novel biomedical applications, e.g. magnetofection, drug targeting or hyperthermia. Among others, the recently developed magnetic measurement technique magnetic particle spectroscopy (MPS) provides signals that are specific for MNP. MPS is based on the non-linear magnetic response of MNP exposed to a strong sinusoidal excitation field of up to 25 mT amplitude and 25 kHz frequency. So far, it has been proven a powerful tool for quantification of MNP in biological systems. In this study we investigated in detail the influence of typical biological media on the magnetic behavior of different MNP systems by MPS. The results reveal that amplitude and shape (ratio of harmonics) of the MPS spectra allow for perceptively monitoring changes in MNP magnetism caused by different physiological media. Additionally, the observed linear correlation between MPS amplitude and shape alterations can be used to reduce the quantification uncertainty for MNP suspended in a biological environment.

## 1. Introduction

The small size of magnetic nanoparticles (MNP) comparable with or even smaller than the organism forming biological cells make them ideally suited for advanced applications in medical diagnostics and therapy [1–5]. Usually, MNP consist of a magnetically active core (e.g. crystallites of iron oxides like magnetite/maghemite) surrounded by an organic shell of appropriate materials (e.g. dextran, citrate, PEG) to provide steric or electrostatic stabilization against attraction (magnetic, van der Waal) of the MNP cores and to maintain colloidal and chemical stability under physiological conditions. Optionally, suitable ligands, antibodies, or proteins can be bound to the MNP surface to enable highly selective biochemical interaction with biological systems.

For biomedical application peculiar magnetic properties of the MNP are exploited, e.g. to separate molecules or cells [6,7], to facilitate the entrance of substances into the cell nucleus in magnetofection [8,9] or the spatially constraint delivery of chemotherapeutics in magnetic drug targeting [10,11]. Furthermore, the heating tissue mediated by MNP exposed to an alternating magnetic field is anticipated in magnetic hyperthermia and thermoablation therapies [12,13]. Recently, the highly sensitive detection of MNP is envisioned in Magnetic Particle Imaging (MPI) [14] or Magnetorelaxometry Imaging [15], which might become valuable diagnostic tools directly probing the MNP without being hampered by background due to

biological tissue.

Each application requires specific physical properties of MNP and maintaining functionality during application (e.g. in vitro or in vivo). Surface structure and charge as well as MNP size are all considered central factors determining applicability, pharmacokinetics, toxicity and biodistribution. Thus, important but challenging issues of MNP characterization and quality control are the measurement and quantification in vitro or in vivo, or in environments mimicking physiological conditions. Magnetic particle spectroscopy (MPS) has been proven an supreme measurement technique to detect MNP in biological samples (tissue or cells) [16–18]. MPS exploits the non-linear dynamic magnetization behavior of MNP and uses the fact, that the signal measured on sinusoidally excited MNP contains odd multiples of the excitation frequency clearly visible after Fourier transformation of the received signal. With a linear relation between MPS signal amplitude and MNP amount (often quoted by the iron amount) over several orders of magnitude down to the nanogram range this technique is ideally suited for specific and accurate MNP quantification even in living cells [19] or in a liquid flow [20]. The quantification relies on the MPS curve of a reference sample of known MNP or iron amount. Basically, MPS signals depend on the magnetic properties of the MNP but may also be influenced by surrounding biological environment possibly causing viscosity changes or aggregation of the MNP [21,22] and thereby changes in the amplitudes of the corresponding MPS

\* Corresponding author.

E-mail address: [norbert.loewa@ptb.de](mailto:norbert.loewa@ptb.de) (N. Löwa).

signals. As a consequence the quantification uncertainty may be seriously increased using a reference sample with MNP in a different state than the MNP in a tissue or cell sample.

The stability of MNP suspensions results from the balance of attractive (magnetic) and repulsive forces. Whereas the magnetic attraction strongly depends on the MNP volume, repulsion can be promoted by MNP shell material causing steric or electrostatic forces. The latter can be derived from the zeta potential  $\zeta$  that is strongly influenced by the ionic strength and pH of the surrounding environment. Thus, charged MNP are prone to precipitate in physiological suspension due to neutralization of the surface charge caused by ionic components in the medium. Additionally, electrostatically stabilized MNP tend to adsorb proteins present in physiological environment through electrostatic interaction which may lead to aggregation [23,24]. However, the specific interactions of MNP with proteins, cell surfaces, intracellular organelles and the complex mechanisms involved are not fully understood and still under investigation [21,25,26]. Therefore, MNP characterization in physiological relevant environment is crucial for understanding the interaction of MNP with biological systems.

In our study we focused on magnetic characterization of MNP using MPS. We characterized different MNP systems as delivered from manufacturers by measuring size, zeta potential and MPS signal behavior in aqueous suspension. In addition, the effect of ionic strength, pH value, incubation time and different physiological media on MPS signal was measured systematically. This allowed us to analyze alterations of the MPS signal caused by interaction of MNP with biological environment. In addition, we demonstrate that by understanding MPS signal alterations one can anticipate the MNP behavior in different environments and to some degree reduce the uncertainty of the MPS quantification procedure.

## 2. Materials and methods

### 2.1. Magnetic nanoparticles

We used 11 different MNP types (including commercially available Resovist<sup>®</sup> and Feraheme<sup>®</sup>) in aqueous suspension all adjusted to the same iron concentration of 50  $\mu\text{mol/L}$  using deionized distilled water ( $\text{ddH}_2\text{O}$ ). Details of origin, coating, and some physical parameters of the MNP are summarized in Table 1. The influence of pH and ionic strength on MPS signal was investigated in detail using the commercial formulations Resovist<sup>®</sup> and Feraheme<sup>®</sup> which differ primarily in size (see Table 1) leading to higher attractive magnetic forces for Resovist<sup>®</sup>.

### 2.2. Suspension media

All chemicals used in this study were of analytical reagent grade.

**Table 1**

Summary of the different MNP types used in this work. Given are the name, the ID used in the graphs together with the name of the supplier and the coating of the MNP. Furthermore, the hydrodynamic diameter  $d_z$  ( $z$ -average) and zeta potential  $\zeta$  obtained by DLS and characteristic MPS parameters  $A_3$  normalized to iron amount and shape parameter  $A_5/A_3$  as determined for the stock suspension are presented. The limit of detection (LOD) was defined as the iron mass of a MNP sample corresponding to a moment  $A_3$  that is three times the standard deviation of  $A_3$  resulting from 20 blank measurements. The numbers in parentheses denote the uncertainty of the last digit. n.d.=not determined.

Name	ID	Supplier	Coating	$d_z$ nm	$\zeta$ mV	$A_3$ A m <sup>2</sup> /kg (Fe)	$A_5/A_3$ %	LOD ng
Feraheme <sup>®</sup>	FER	AMAG Pharmaceuticals	Carbohydrate	30.2(7)	-29(2)	0.75(1)	14.64(1)	13.4(2)
Resovist <sup>®</sup>	RES	Bayer HealthCare	Carboxy dextran	58.3(1)	-18.2(6)	8.67(3)	38.38(2)	1.153(4)
SHP20	S20	Ocean Nanotech	Carboxylic acid	57.2(4)	-40(5)	9.24(8)	30.93(1)	1.08(1)
SHP25	S25	Ocean Nanotech	Carboxylic acid	46.2(1)	-34(3)	18.29(8)	30.8(1)	0.547(2)
SOMag5	SOM	LMU Munich	Silicon oxide	104.6(4)	-25.8(7)	4.74(1)	29.09(1)	2.11(1)
VSOP F15	F15	Charité	Citrate	24.5(2)	-50(19)	0.92(1)	17.58(2)	10.81(8)
VSOP F16	F16	Charité	Citrate	22.5(7)	-26(5)	0.22(1)	9.20(3)	45.1(3)
CapsMag 0	CM0	Magneticfluids	None	101.5(6)	19.2(7)	3.07(6)	27.91(1)	3.25(6)
CapsMag Citrat L	CML	Magneticfluids	Citrate	102.3(6)	-16.7(7)	4.5(1)	23.34(4)	2.21(5)
CapsMag Citrat S	CMS	Magneticfluids	Citrate	70.9(4)	-30.1(9)	5.83(3)	30.81(2)	1.72(1)
USPIO	USP	Magneticfluids	Carboxy-methylated dextran	35.8(2)	n.d.	2.81(9)	26.91(2)	3.5(1)

Eight different MNP environments (media) were supplied by solutions of  $\text{ddH}_2\text{O}$ , bovine serum albumin (BSA, Sigma Aldrich, Germany), glycerol 85% (Otto Fischer, Germany), sodium chloride (NaCl, Merck, Germany), sodium hydroxide (NaOH), nitric acid 0.65% ( $\text{HNO}_3$ ), hydrochloric acid (HCl, all Carl Roth, Germany), and EDTA stabilized human blood. Glycosaminoglycans (GG) were extracted according to the procedure presented by Ludwig et al. [27] from THP-1 cells which are known to synthesize large amounts of membrane-bound and extracellular proteoglycans. pH values were adjusted by using solutions of NaOH or HCl, as necessary. Furthermore, we used sodium silicate solution ( $\text{SiO}_2$   $\text{Na}_2\text{O}$ , Carl Roth, Germany) as silica is one of the naturally occurring substance in living systems and thus a potential candidate for biomaterial applications [28].

### 2.3. Colloidal characterization

Dynamic light scattering (DLS) was used to measure the MNP surface charge  $\zeta$  in neutral aqueous solution as well as the hydrodynamic size  $d_z$  of the samples. Therefore, a Zetasizer Nano-ZS device (Malvern U.K.) equipped with a green laser operating at a wavelength of 633 nm was employed (detection angle 173°). The same device was used to derive the  $\zeta$  potential from the Smoluchowski's approximation by measuring the electrophoretic mobility of the MNP. All measurements were performed at 21 °C.

### 2.4. Magnetic Particle Spectroscopy (MPS)

Originally MPS was developed to quantify the suitability of MNP for the imaging modality MPI. MPS is based on the detection of the non-linear magnetic susceptibility of MNP [14]. For this purpose a sinusoidal excitation field  $B_{\text{ex}}=25$  mT at a frequency  $f_0=25$  kHz is applied to an MNP sample. Due to the inherent non-linearity of the magnetization curve the measured response of the MNP contains odd multiples of  $f_0$  (i.e. higher harmonics).

We used a commercial Magnetic Particle Spectrometer (MPS-3, Bruker, Germany). For the measurement a sample volume of 20  $\mu\text{L}$  is filled into a PCR cup and placed in the pick-up coil of the MPS system. The sample chamber is tempered to 36.6 °C. Typically the induced magnetization of the MNP response in the pick-up coil is amplified after filtering to remove the fundamental excitation frequency  $f_0$  and recorded over a time interval of 10 s. By Fourier transformation the spectral components show distinct amplitudes  $A_n$  at odd multiples  $n$  of the drive frequency  $f_0$  as can be seen in Fig. 1. In order to determine the noise floor and the uncertainty of the harmonic amplitudes MPS signals of a blank sample were recorded 100 times and the standard deviation was calculated. For the third harmonic amplitude  $A_3$  a residual moment of  $5 \cdot 10^{-12}$  A m<sup>2</sup> was determined showing the high sensitivity of the MPS device.

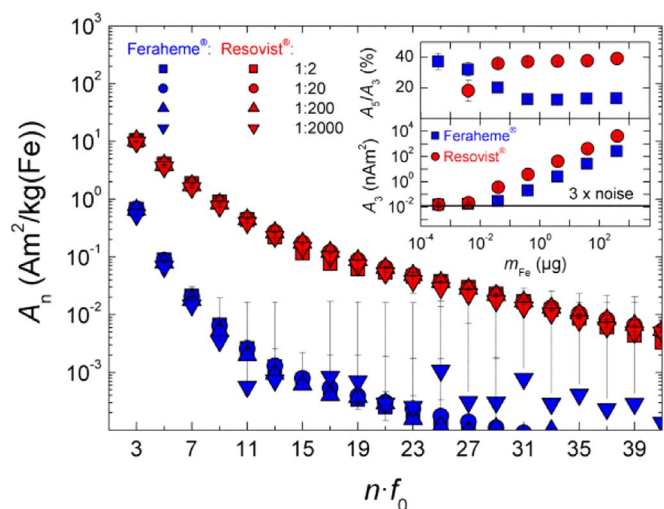


**Fig. 1.** MPS signal amplitudes  $A_n$  of different dilutions (1:2 to 1:2000) of Resovist<sup>®</sup> and Feraheme<sup>®</sup> measured at  $B_{ex}=25$  mT. The MPS signal amplitudes  $A_n$  were normalized to the respective iron amount. Inset: Serial dilution of MNP (1:2 to 1:2000) in ddH<sub>2</sub>O showing the linear relation of MPS signal amplitude  $A_3$  and MNP amount (iron content). The horizontal line shows the threefold standard deviation of 20 blank measurements. The shape of the MPS spectrum (also represented by the  $A_5/A_3$  ratio) is not affected by dilution in the investigated dilution range. This indicates that the dynamic magnetic behavior of the MNP remains constant.

We used the third harmonic amplitude  $A_3$  and the harmonic ratio  $A_5/A_3$  (representing the shape of the spectrum) to assess changes of the MPS signal due to the influence of different environments.

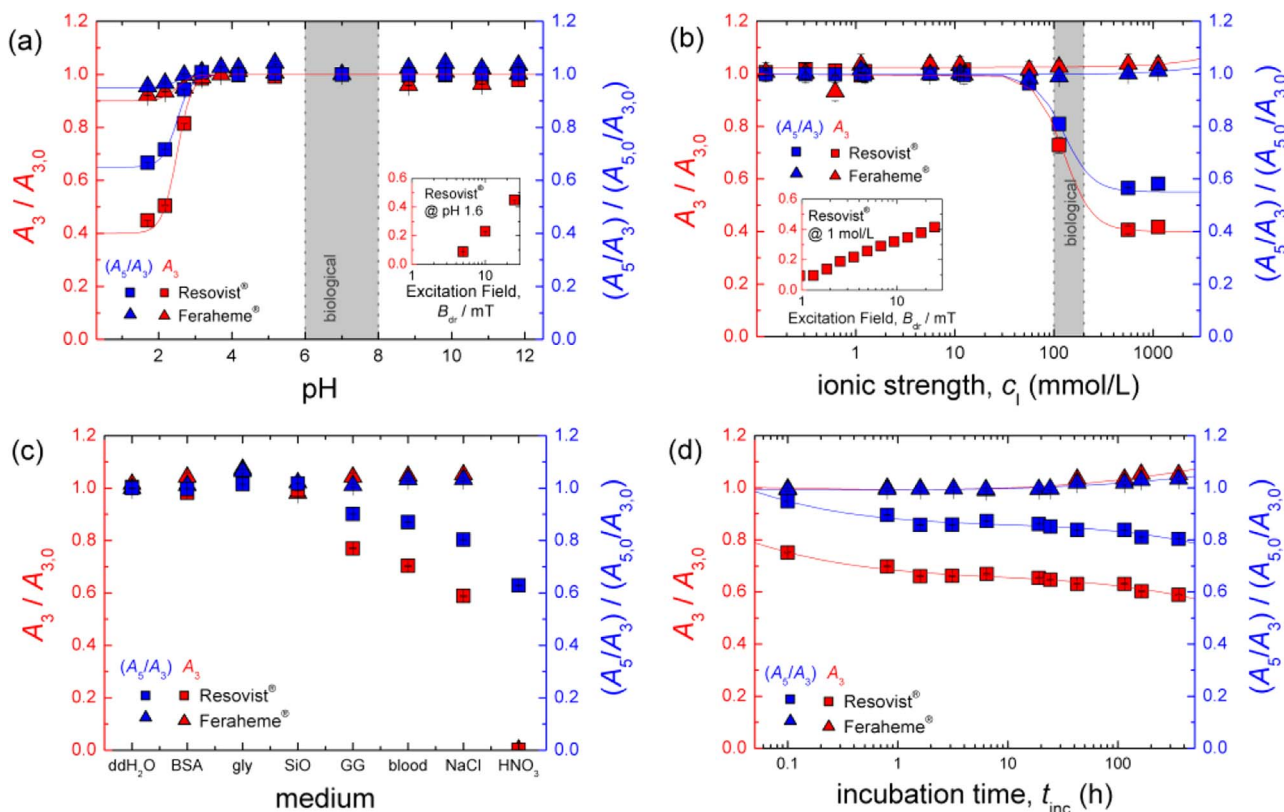


**Fig. 2.** Behavior of Resovist<sup>®</sup> (squares) and Feraheme<sup>®</sup> (triangles) in different media as seen by MPS. Unless otherwise stated, all MPS measurements were performed at  $B_{ex}=25$  mT 1 h after incubation of MNP with the respective medium. The red symbols denote the change of MPS signal amplitude  $A_3$  with respect to the value before incubation  $A_{3,0}$ . The shape of the MPS spectra, represented by the  $A_5/A_3$  ratio, is also related to the value before incubation (blue symbols). The solid lines are sigmoidal fits to guide the eye. (a) Influence of varying pH-values of the surrounding environment on MPS signal. The grey area covers the range of pH values to be found in biological systems. (b) Influence of varying medium ionic strength  $c_i$  on MPS signal. The grey area covers the range of ionic strength to be found in biological systems. (c) Influence of varying media on MPS signal. (d) Influence of time  $t_{inc}$  after diluting MNP in NaCl solution (154 mmol/L) on MPS signal. (For interpretation of the references to color in this figure legend, the reader is referred to the web version of this article.)

### 2.5. Incubation

First the MPS signal of 5  $\mu$ L of the pure MNP solution, corresponding to an iron amount of 14  $\mu$ g, was recorded to obtain the initial value for amplitude  $A_{3,0}$  and shape  $A_{5,0}/A_{3,0}$  of the MPS spectra of each MNP sample. Afterwards, 25  $\mu$ L of the corresponding medium solution were added and the MPS signals were measured after 0.1 h, 0.8 h, 1.6 h, 3 h, 6 h, 19 h, 24 h, 42 h, 115 h, 160 h, and 350 h to determine MPS signal changes. Furthermore, ionic strength- and pH-dependent aggregations of the MNP were measured over a wide range of medium concentrations (pH: 1.7, 2.2, 2.7, 3.2, 4.2, 5.2, 8.8, 9.8, 10.8, 11.8, and 12.8; ionic strength: 0.001 mol/L, 0.006 mol/L, 0.01 mol/L, 0.06 mol/L, 0.1 mol/L, 0.6 mol/L, and 1 mol/L) 1 h after incubation of MNP with the corresponding medium.

## 3. Results

### 3.1. Characterization of MNP suspensions

The properties of the MNP suspensions are summarized in Table 1. From DLS measurements we determined the z-average hydrodynamic diameter  $d_z$  for each MNP type in the initial state. We determined the limit of detection (LOD) by measuring the MPS spectra of a serial dilution of MNP at  $B_{excit}=25$  mT. Therefore, the measured MPS signal of the third harmonic  $A_3$  is plotted against nominal iron amount which results in linear calibration curves over more than five orders of magnitude as shown in the lower inset of Fig. 1. From the intersection point of the calibration curve with the horizontal  $A_3$  noise floor of  $1.6 \cdot 10^{-11}$  A m<sup>2</sup> (threefold standard deviation of 20 blank measurements) we estimated the LOD (see Table 1). Additionally, the shape of the MPS

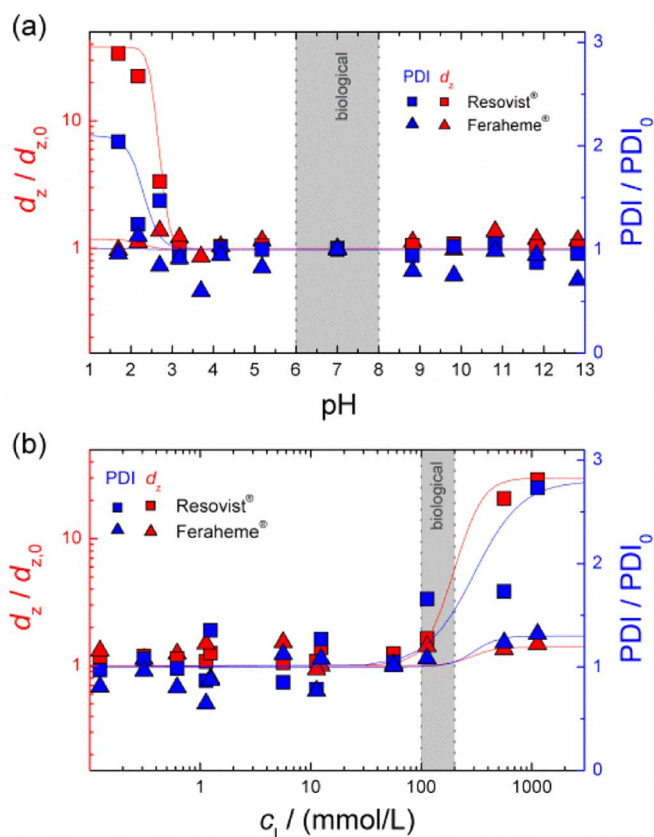


**Fig. 3.** (a) pH- and (b) ionic strength-dependent aggregation of Resovist® (squares) and Feraheme® (triangles) measured by DLS over a wide range of medium concentrations (pH: 1.7–12.8; ionic strength: 0.001–1 mol/L) 1 h after incubation with the respective medium. The hydrodynamic size  $d_z$  (z-average diameter) normalized to the initial (non-aggregated) value  $d_{z,0}$  (red symbols) and the normalized distribution width  $PDI/PDI_0$  (blue symbols) are shown. (For interpretation of the references to color in this figure legend, the reader is referred to the web version of this article.)

spectrum is independent on iron amount in the investigated dilution range, but a characteristic feature of the magnetic properties of the individual MNP system (e.g. distribution of size, anisotropy and composition). Taking the  $A_5/A_3$  ratio as a representative value for the decay of the MPS spectrum no changes were observed for the measured serial dilutions (for Feraheme® and Resovist® see upper inset of Fig. 1).

Zeta potential measurements at pH 7 showed that CM0 was positively charged while all other MNP samples had an anionic surface charge below  $-15$  mV.

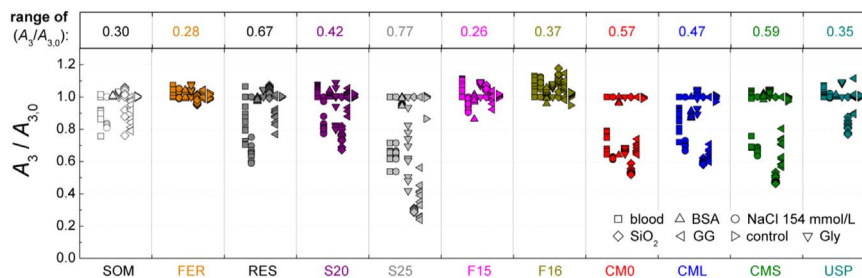


**Fig. 4.** Behavior of the 11 different MNP types ( $m(Fe)=14 \mu g$ ) in different media measured by MPS at  $B_{ex}=25$  mT. Each field shows the amplitude changes  $A_3$  (normalized to amplitude  $A_{3,0}$  of the sample before incubation) after incubation by seven particular media (each drawn as an individual column, identical symbols denote different time points of the measurement after incubation ranging from 0.1h to 360 h). As media have been used (columns from left to right in each field) blood (squares), BSA (triangles up), NaCl (circles),  $SiO_2$  (diamonds), GG (triangle left), control (triangle right), and Gly (triangle down).

### 3.2. Influence of pH

Decreasing the pH of the surrounding medium resulted in a decrease of the normalized MPS amplitude  $A_3/A_{3,0}$  of Resovist®. As it can be seen in Fig. 2a, the MPS signal amplitude reduced significantly in acidic environment below pH 3 by up to 60%. Similarly, the normalized shape factor  $(A_5/A_3)/(A_{5,0}/A_{3,0})$  decreased, albeit to a less marked degree (reduction up to 35%). The measured hydrodynamic diameters  $d_z$  of the MNP solutions demonstrate that strong aggregation occurred at lower pH-values accompanied by broadening particle size distributions (see PDI in Fig. 3a). In highly alkaline solutions no MPS signal alterations were observed and for Feraheme® generally no major negative or positive effects of different pH-values on MPS signals as well as particle size were found.

All negatively charged MNP samples were stable at pH around 7 which is the predominant value under biological conditions (pH 6–8) [29]. At lower pH values (below pH 3) hydrogen ions neutralize the negative surface charge (isoelectric point,  $\zeta=0$  mV) facilitating aggregation of electrostatically stabilized MNP, whereby additionally dissolution of the iron oxide might occur. In contrast MNP carrying positive charges showed the opposite effect. CM0 was stable at around pH 3 and aggregated at higher pH values due to deprotonation.

### 3.3. Influence of ionic strength

The same behavior was found for varying ionic strength as shown in Fig. 2b. Whereas for Feraheme® MPS signals did not change compared to its initial state, the MPS signal of Resovist® decreased with increasing ionic strength. Here, we identified the same trend for the decrease of the MPS signal shape  $A_5/A_3$  but less pronounced compared to the amplitude  $A_3$ . This was also accompanied by an increase of hydrodynamic size  $d_z$  and distribution width (PDI) as measured by DLS (see Fig. 3b). At physiological ionic strength  $c_1=150$  mmol/L no increase of mean hydrodynamic size  $d_z$ , but a significant MPS signal reduction ( $\sim 20\%$ ) and a broader size distribution ( $PDI/PDI_0=1.7$ ) was measured.

In the range of physiologically reasonable conditions ( $c_1=100$ – $200$  mmol/L) the MNP magnetism as detected by MPS may be much more influenced by alterations in the ionic strength. This was supported by other MNP systems investigated here (e.g. see Fig. 4).

### 3.4. Influence of drive field strength

Performing MPS measurements at reduced excitation field amplitudes  $B_{ex}$  (down to 1 mT) revealed that the MPS signal losses observed even became greater at low pH-values and high ionic strength as can be seen in the insets of Fig. 2a and b. For Resovist® dissolved in 1 mol/L NaCl solution the  $A_3$  signal loss increased from 60% measured at  $B_{ex}=25$  mT up to 90% at  $B_{ex}=1$  mT. In contrast, a signal loss of 90% in highly acidic environment (pH 1.6) was measured at  $B_{ex}=5$  mT.

From this the recommendation can be drawn that the quantification of Resovist® by MPS is most reliable at the highest excitation field  $B_{\text{ex}}=25$  mT.

### 3.5. Influence of complex media

These experiments were carried out to evaluate the effect of different surrounding environments on the MPS signal of MNP. The results for Resovist® and Feraheme® are presented in Fig. 2c showing the normalized MPS amplitude loss and the alteration of the MPS signal shape 350 h after incubation with the medium. For Feraheme® no significant signal loss was observed and the shape of the MPS spectrum remains constant with respect to uncertainty. On the contrary, for Resovist® dissolved in GG, blood, and physiological NaCl solution (154 mmol/L)  $A_3$  decreased by 20% up to 40%. Again,  $A_5/A_3$  reduced in the same ratio but less pronounced (10% up to 20%) compared to  $A_3$ . The strongest signal loss was observed in 0.65% HNO<sub>3</sub> (pH 1) where  $A_3$  corresponds only to 0.03% of  $A_{3,0}$ . In contrast to the observations in NaCl solutions the shape of the MPS signal  $A_5/A_3$  decreased noticeably less. This might be due to the fact, that some MNP already were completely dissolved whereas other MNP were intact possibly due to a more resistant coating. In ddH<sub>2</sub>O, BSA, glycerol, and sodium silicate solutions the MPS signals remain stable within measurement uncertainty.

The results for all MNP systems investigated here are shown in Fig. 4. It can be seen, that the extent of the MPS signal alteration induced by complex environments strongly depends on MNP type and can have stabilizing (S20 in blood) or adverse (S25 in blood) effects.

### 3.6. Influence of incubation time

The influence of incubation time on the MPS signal of Resovist® in physiological NaCl solution (154 mmol/L) is presented in Fig. 2d. As it can be seen, the amplitude  $A_3$  and the shape  $A_5/A_3$  both decreased with the same rate but with an offset of around 20% for  $A_3$ . After 350 h  $A_3$  decreased by 40% and  $A_5/A_3$  correspondingly less (around 20%). For Feraheme® no signal alteration was measured during the observation time.

The MPS signal alteration of MNP in biological environments might be time dependent which should be considered for MNP quantification as well as for comparative aggregation studies.

### 3.7. Impact on quantification uncertainty

The results obtained for all MNP systems in different environments are summarized in Fig. 4 showing the  $A_3$  signal loss measured in each medium during all time points over a period of 350 h. The iron amount of all MNP samples was 14 µg(Fe). It can be seen, that the larger MNP (Resovist®, S20, S25, CM0, CML, and CMS) are stronger affected by medium variation. For small sized MNP (Feraheme®, F15, F16, and USP) the range of  $A_3$  variation was below 40%. Only for large sized SOM particles (with  $d_z=104.6$  nm), which are stabilized by silicon oxide,  $A_3$  changed only by 30%. The strongest signal change in different environments with 77% and 67% was measured for S25 and Resovist®, respectively, which both exhibit resembling high MPS signal amplitudes ( $A_3=18$  mA m<sup>2</sup>/g(Fe) and 9 mA m<sup>2</sup>/g(Fe)) and flat spectra ( $A_5/A_3=31\%$  and 38%) in initial state. These signal variation should be incorporated into the uncertainty budget in reference sample based quantification of MNP in different environments using MPS.

Remarkably, the comparison of the MPS amplitude  $A_3$  loss for all MNP systems with their respective normalized shape  $A_5/A_3$  showed a universal linear correlation ( $R^2=0.85$ ) with a slope of 1.24 (see red line in Fig. 5). With the knowledge of this generalized MPS signal behavior including  $A_5/A_3$  the range of  $A_3$  variation reduced to 39%. This value could be decreased below 20% down to 4% if each MNP system was evaluated individually (see grey line in Fig. 5 for S25). With this

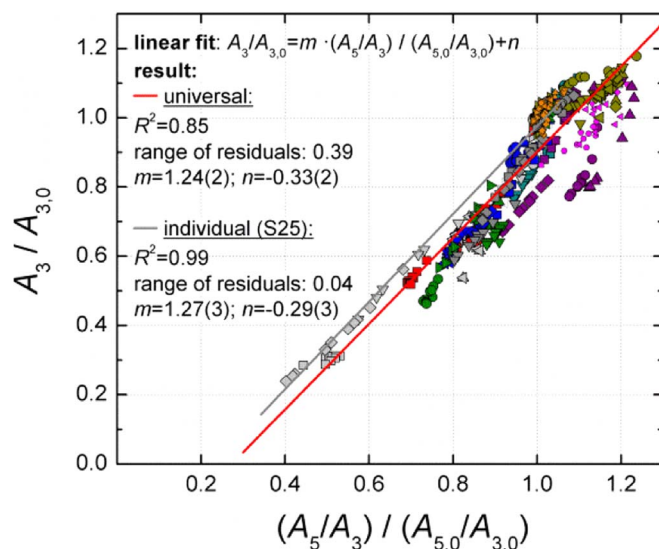


**Fig. 5.** Correlation between MPS signal amplitude  $A_3$  and shape  $A_5/A_3$  of the 11 different MNP types ( $m(\text{Fe})=14$  µg) in different media measured by MPS at  $B_{\text{ex}}=25$  mT. The symbol assignment corresponds to Fig. 4 where symbol color and shape assign MNP type and medium, respectively. Identical symbols denote different time points after incubation ranging from 0.1h to 350 h. A linear fit was applied to measured MPS signals considering all media at all time points for all MNP types (red line) as well as for each individual MNP type (e.g. S25 grey line) to evaluate the correlation between  $A_3$  and  $A_5/A_3$ . (For interpretation of the references to color in this figure legend, the reader is referred to the web version of this article.)

correlation the quantification uncertainty can be reduced if MNP aggregation in different environments is anticipated. Note, that HCl and HNO<sub>3</sub> were not considered for the correlation of MPS amplitude and shape as, besides aggregation, these media also dissolve MNP which results in bad correlation results.

## 4. Conclusions

In the present study we introduced MPS to provide a highly sensitive and specific technique for the quantification of MNP by measuring MNP signals without any background contribution. This is a decisive advantage over conventional light scattering techniques (e.g. dynamic light scattering) typically used to study nanoparticles in physiological environments, whereas MPS is not limited to transparent media. Furthermore, MPS provides reliable quantification results over a wide range of MNP concentrations if the dynamic magnetic behavior of the MNP does not change. Depending on the magnetic properties of the nanoparticles, the relative iron amount of MNP could be resolved down to the lower nanogram range in small sample volumes (5 µL). A further essential feature which is important for MNP quantification is the linear characteristic calibration curve for each MNP system. One benefit of this method is that any alteration of the dynamic magnetic behavior can be quantified by analyzing the MPS signal shape (e.g.  $A_5/A_3$  ratio). Through a series of aggregation experiments, we demonstrated that the MPS signal amplitude of an MNP sample at constant material amount may greatly vary in different environments (pH, ionic strength, viscosity) and additionally, can be time dependent. With regard to reference sample based MNP quantification (at  $B_{\text{ex}}=25$  mT) this leads to an increased uncertainty of 15% up to 77% depending on MNP type and which significantly grows at lower MPS excitation fields  $B_{\text{ex}}$ .

Interestingly, we found a correlation between changes of MPS amplitude  $A_3$  and shape  $A_5/A_3$  allowing for a subsequent correction of the specific amplitude  $A_3$  used for quantification. With this procedure the quantification uncertainty could be reduced below 20% for all MNP systems. Furthermore, our results revealed that  $A_3$  and  $A_5/A_3$  normalized to the values of the sample as supplied ( $A_{3,0}$  and  $A_{5,0}/A_{3,0}$ ) provide

an universal correlation for all MNP types. The residual uncertainty for quantification mounted to 40%. Nevertheless, where highest accuracy is required it is recommended to measure the MPS signal as a function of concentration in the corresponding medium, to confirm linearity.

Our results demonstrate that MPS is a powerful tool to monitor the behavior of MNP in different physiological media. Both parameters, amplitude  $A_3$  and harmonic ratio  $A_5/A_3$  allow for a sensitive and specific detection of changes caused by the interaction of MNP with surrounding physiological environment. Furthermore, the high linear correlation between MPS amplitude and harmonic ratio alterations enables the reduction of quantification uncertainty for MNP in a biological environment.

### Acknowledgment

This research was supported by German Research Foundation (research group FOR917, Nanoguide TR408/7-2) and EU-FP7 (NanoMAG grant no 604448).

### References

- [1] A.K. Gupta, M. Gupta, Synthesis and surface engineering of iron oxide nanoparticles for biomedical applications, *Biomaterials* 26 (2005) 3995–4021.
- [2] Q.A. Pankhurst, et al., Applications of magnetic nanoparticles in biomedicine, *J. Phys. D.: Appl. Phys.* 36 (2003) R167–R181.
- [3] L. Trahms, Springer, Berlin Heidelberg, 2009, pp. 1–32. doi: [http://dx.doi.org/10.1007/978-3-540-85387-9\\_5](http://dx.doi.org/10.1007/978-3-540-85387-9_5).
- [4] K.M. Krishnan, Biomedical nanomagnetism: a spin through possibilities in imaging, diagnostics, and therapy, *IEEE Trans. Magn.* 46 (2010) 2523–2558.
- [5] P. Tartaj, et al., The preparation of magnetic nanoparticles for applications in biomedicine, *J. Phys. D.: Appl. Phys.* 36 (2003) R182–R197.
- [6] H.H. Yang, et al., Magnetite-containing spherical silica nanoparticles for biocatalysis and bioseparations, *Anal. Chem.* 76 (2004) 1316–1321.
- [7] I.S. Lee, et al., Ni/NiO core/shell nanoparticles for selective binding and magnetic separation of histidine-tagged proteins, *J. Am. Chem. Soc.* 128 (2006) 10658–10659.
- [8] C. Plank, et al., The magnetofection method: using magnetic force to enhance gene delivery, *Biol. Chem.* 384 (2003) 737–747.
- [9] O. Mykhaylyk, et al., Recent advances in magnetofection and its potential to deliver siRNAs in vitro, *Methods Mol. Biol.* 487 (2009) 111–146.
- [10] C. Alexiou, et al., Delivery of superparamagnetic nanoparticles for local chemotherapy after intraarterial infusion and magnetic drug targeting, *Anticancer Res.* 27 (2007) 2019–2022.
- [11] B. Polyak, G. Friedman, Magnetic targeting for site-specific drug delivery: applications and clinical potential, *Expert Opin. Drug Deliv.* 6 (2009) 53–70.
- [12] A.P. Khandhar, R.M. Ferguson, J.A. Simon, K.M. Krishnan, Tailored magnetic nanoparticles for optimizing magnetic fluid hyperthermia, *J. Biomed. Mater. Res. A* 100 (2012) 728–737.
- [13] I. Hilger, R. Hergt, W.A. Kaiser, Effects of magnetic thermoablation in muscle tissue using iron oxide particles: an in vitro study, *Investig. Radiol.* 35 (2000) 170–179.
- [14] B. Gleich, J. Weizenecker, Tomographic imaging using the nonlinear response of magnetic particles, *Nature* 435 (2005) 1214–1217.
- [15] M. Liebl, U. Steinhoff, F. Wiekhorst, J. Hauelsen, L. Trahms, Quantitative imaging of magnetic nanoparticles by magnetorelaxometry with multiple excitation coils, *Phys. Med. Biol.* 59 (2014) 6607–6620.
- [16] N. Löwa, et al., Cellular uptake of magnetic nanoparticles quantified by magnetic particle spectroscopy, *IEEE Trans. Magn.* 49 (2013) 275–278.
- [17] J.W.M. Bulte, et al., Quantitative 'Hot Spot' imaging of transplanted stem cells using superparamagnetic tracers and Magnetic Particle Imaging (MPI), *Tomogr. – J. imaging Res.* 1 (2015) 91–97.
- [18] C. Gräfe, et al., Magnetic particle spectroscopy allows precise quantification of nanoparticles after passage through human brain microvascular endothelial cells, *Phys. Med. Biol.* 61 (2016) 3986–4000.
- [19] W.C. Poller, et al., Magnetic particle spectroscopy reveals dynamic changes in the magnetic behavior of very small superparamagnetic iron oxide nanoparticles during cellular uptake and enables determination of cell-labeling efficacy, *J. Biomed. Nanotechnol.* 12 (2016) 337–346.
- [20] N. Löwa, P. Radon, D. Gutkelch, R. August, F. Wiekhorst, Hyphenation of field-flow fractionation and magnetic particle spectroscopy, *Chromatography* 2 (2015) 655–668.
- [21] H. Arami, R.M. Ferguson, A.P. Khandhar, K.M. Krishnan, Size-dependent ferrohydrodynamic relaxometry of magnetic particle imaging tracers in different environments, *Med. Phys.* 40 (2013) 071904.
- [22] T. Wawrzik, T. Yoshida, M. Schilling, F. Ludwig, Debye-based frequency-domain magnetization model for magnetic nanoparticles in magnetic particle spectroscopy, *IEEE Trans. Magn.* 51 (2015) 1–4.
- [23] Z.P. Chen, et al., Stability of hydrophilic magnetic nanoparticles under biologically relevant conditions, *J. Nanosci. Nanotechnol.* 8 (2008) 6260–6265.
- [24] U. Sakulku, et al., Protein corona composition of superparamagnetic iron oxide nanoparticles with various physico-chemical properties and coatings, *Sci. Rep.* 4 (2014) 5754–5756.
- [25] G. Shahnaz, et al., Efficient MRI labeling of endothelial progenitor cells: design of thiolated surface stabilized superparamagnetic iron oxide nanoparticles, *Eur. J. Pharm. Biopharm.* 85 (2013) 346–355.
- [26] U. Sakulku, M. Mahmoudi, L. Maurizi, J. Salaklang, H. Hofmann, Protein corona composition of superparamagnetic iron oxide nanoparticles with various physico-chemical properties and coatings, *Sci. Rep.* 4 (2014) 5020.
- [27] A. Ludwig, et al., Rapid binding of electrostatically stabilized iron oxide nanoparticles to THP-1 monocytic cells via interaction with glycosaminoglycans, *Basic Res. Cardiol.* 108 (2013) 15–17.
- [28] R. Viitala, S. Areva, M. Jokinen, M. Koskinen, NATO Science for Peace and Security Series C: Environmental Security, Springer, Netherlands, 2008, pp. 251–268. [http://dx.doi.org/10.1007/978-1-4020-8514-7\\_15](http://dx.doi.org/10.1007/978-1-4020-8514-7_15).
- [29] I.F. Tannock, D. Rotin, Acid pH in tumors and its potential for therapeutic exploitation, *Cancer Res.* 49 (1989) 4373–4384.